Post print of accepted manuscript in *Environ. Sci. Tech.* doi: 10.1021/acs.est.3c07851

Supplementary Information (SI) for

Deforestation as an anthropogenic driver of mercury pollution

Aryeh Feinberg[a]*, *Martin Jiskra*[b]*, *Pasquale Borrelli*[c], *Jagannath Biswakarma*[b,d], *and Noelle E. Selin*[a,e]

[a] Institute for Data, Systems, and Society, Massachusetts Institute of Technology, Cambridge, MA 02139, USA

[b] Environmental Geosciences, University of Basel, Basel 4056, Switzerland

[c] Department of Science, Roma Tre University, Rome 00146, Italy

[d] Department of Water Resources and Drinking Water, Eawag, Dübendorf 8600, Switzerland

[e] Department of Earth, Atmospheric, and Planetary Sciences, Massachusetts Institute of Technology, Cambridge, MA 02139, USA

*Correspondence to: arifeinberg@gmail.com (A.F.); martin.jiskra@gmail.com (M.J.)

Number of pages: 19

Number of figures: 11

Number of tables: 6

Section S1. Soil emissions parameterization

We improved the model's parametrization of Hg^0 soil emissions by adopting a new formulation for the parametrization, suggested by Khan et al.[1]:

$$E_{\text{soil}} = aC^b R_g^c \qquad \text{(Eq. S1)}$$

where E_{soil} are soil emissions (ng m^{-2} h^{-1}), C is the concentration of Hg in soils (µg g^{-1}), R_g is the solar radiation flux at the ground (W m^{-2}), and a, b, and c are coefficients.

As in Selin et al.[2], the solar radiation atwi ground (R_g) is determined by considering attenuation of the solar radiation flux (R_S) by shading from the overhead canopy, parametrized by the leaf area index (LAI):

$$R_g = R_S \exp\left(-\frac{\alpha \text{LAI}}{\cos\theta}\right) \qquad \text{(Eq. S2)}$$

where $\alpha = 0.5$, assuming extinction from a random angular distribution of leaves[3] and θ is the solar zenith angle.

We compiled several relevant observational constraints for the parametrization in Tables S1 and S2. Observational studies from the Amazon region suggest that deforestation has a large impact on soil emissions due to removal of canopy shading, showing factors of 1.8×, 6.7×, and >31× more emissions in forested compared to deforested land plots (Table S1). Observational studies from other regions find a similarly high sensitivity of soil emissions to the presence of forest: open fields in China showed 6–10 times higher Hg emissions than forests[4] and logging in the US flipped the surface-air Hg^0 flux from net deposition to net emissions (-2.2 µg m^{-2} yr^{-1} to +5.5 µg m^{-2} yr^{-1}) [5]. For extratropical grassland soil emissions, we use the compiled median values from Zhu et al.[6] and Agnan et al.[7]

We conducted a parameter sweep of a, b, and c, calculating globally-gridded soil emissions using annual solar radiation data (Fig. S1). Sensitivity simulations showed that the ratio of deforested to forested soil emissions in the Amazon (median value 6.7) can tune the exponent for the radiation term (c in Eq. S1), i.e., the response of emissions to canopy shading. The exponent for the soil concentration term (b) was tuned with the ratio of deforested Amazon soil emissions (Table S1) to extratropical grassland soil emissions from the Northern Hemisphere from two review studies[6,7] (overall Amazon to extratropical ratio of 5.3). Lastly, after these coefficients are tuned, the prefactor a is adjusted so that predicted annual mean emissions match the observed median magnitudes of Amazon deforested soil emissions (23 µg m^{-2} yr^{-1}) and extratropical grassland emissions (4.3 µg m^{-2} yr^{-1}).

We recognize the uncertainties in the observed data used to tune this parametrization, and thus we constructed 100 alternative parametrizations that fit within observed data bounds (Table S5). These parametrizations were applied in offline uncertainty analyses to assess 95% confidence intervals in the fluxes driven by deforestation (Section S4).

Table S1. Literature review of available Hg^0 soil emission flux measurements from the Amazon region, differentiated by land cover type.

Reference	Location	Site	Deforested Hg^0 flux ($\mu g\ m^{-2}\ yr^{-1}$)	Forested Hg^0 flux ($\mu g\ m^{-2}\ yr^{-1}$)	Flux ratio (deforest:forest)
Magarelli and Fostier[8]	Negro River Basin, Brazil	#1	27 ± 9	0.6 ± 1.5	
		#2	19	–1.0 ± 0.8	
		#3	9.8 ± 0.7		
		Mean	18	–0.2	> 31[a]
Almeida et al.[9]	Rondônia, Brazil	#1	79 ± 110	44 ± 18	1.8
Carpi et al.[10]	Acre, Brazil	#1	19 ± 2	2.9 ± 0.8	6.7
		#2	230[b]		
	Median		**23**	**1.8**	**6.7**

[a]lower limit calculated assuming the forested flux is equal to site #1, as site #2 shows negative overall flux; deforested flux assumed as mean.

[b]this site was 2-months post-fire and soil temperatures were still elevated; this flux is excluded from ratio calculations

Table S2. Observational constraints used to tune the soil emissions parametrization.

Constraint	Value	Reference	Coefficient constrained
Amazon deforested soil emissions ($\mu g\ m^{-2}\ yr^{-1}$)	23	Table S1	*a*
Extratropical grassland soil emissions ($\mu g\ m^{-2}\ yr^{-1}$)	4.3[†]	Zhu et al.[6]; Agnan et al.[7]	*a*
Ratio of Amazon to extratropical soil emissions	5.3	(23:4.3)	*b*
Ratio of deforested to forested Amazon soil emissions	6.7	Table S1	*c*

[†]average of grassland median Hg^0 fluxes from the two independent review studies

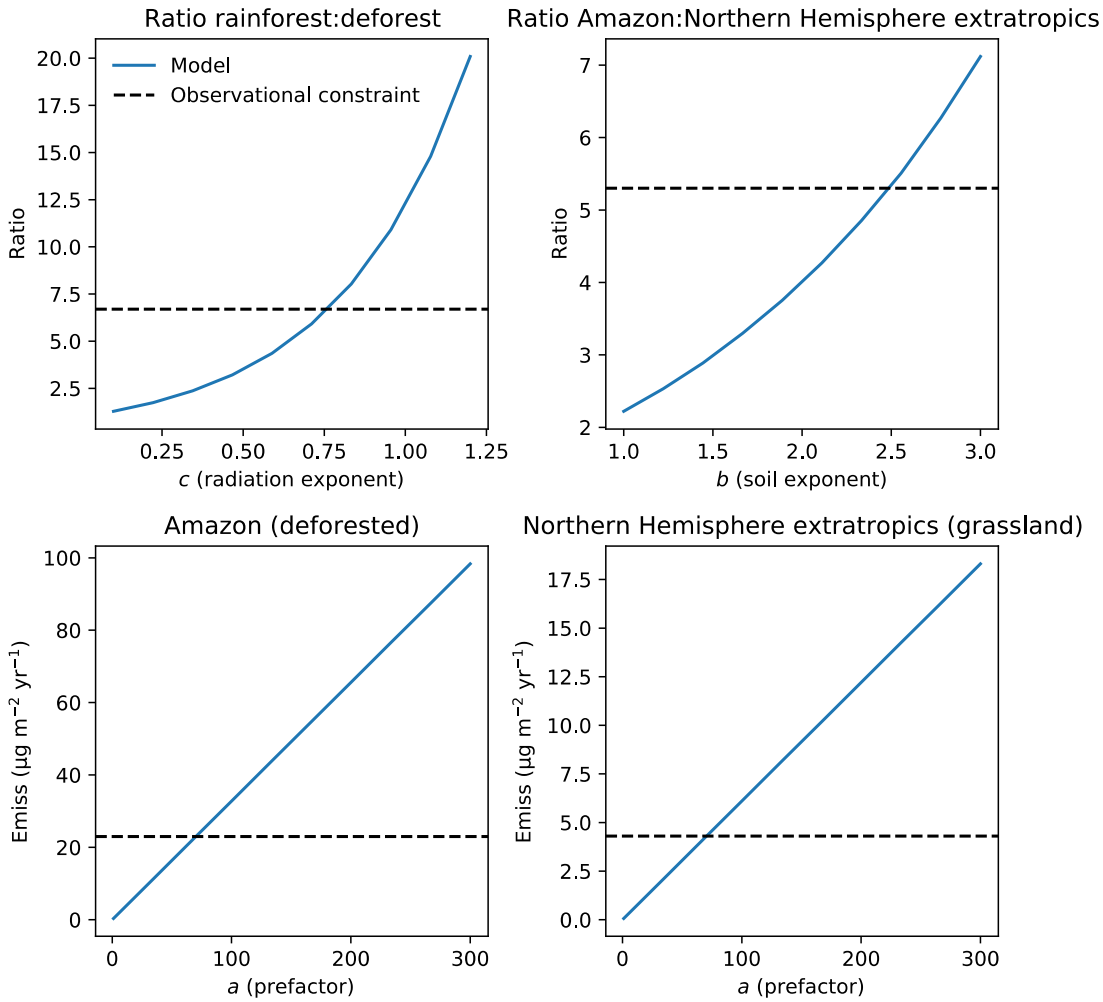

Figure S1. Parameter tuning (Eq. S1) to match observational constraints from Table S2.

The tuning procedure is illustrated in Fig. S1, yielding best matches for $a = 71$, $b = 2.5$, and $c = 0.76$. We compare the gridded annual mean soil emissions from the previous soil emission parametrization (GEOS-Chem v12.8) and the current study (Eq. S1) in Fig. S2. Global annual mean soil Hg^0 emissions in the new parametrizations (954 Mg yr^{-1}) is similar to the predictions from two GEOS-Chem studies[11,12] using the previous parametrization: 860 ± 440 Mg yr^{-1} and 910 Mg yr^{-1}. The spatial distribution of emissions (Fig. S2) shows a decrease in vegetated regions (e.g., the Amazon and Congo rainforests) and an increase in regions with high soil Hg concentrations (e.g., eastern China).

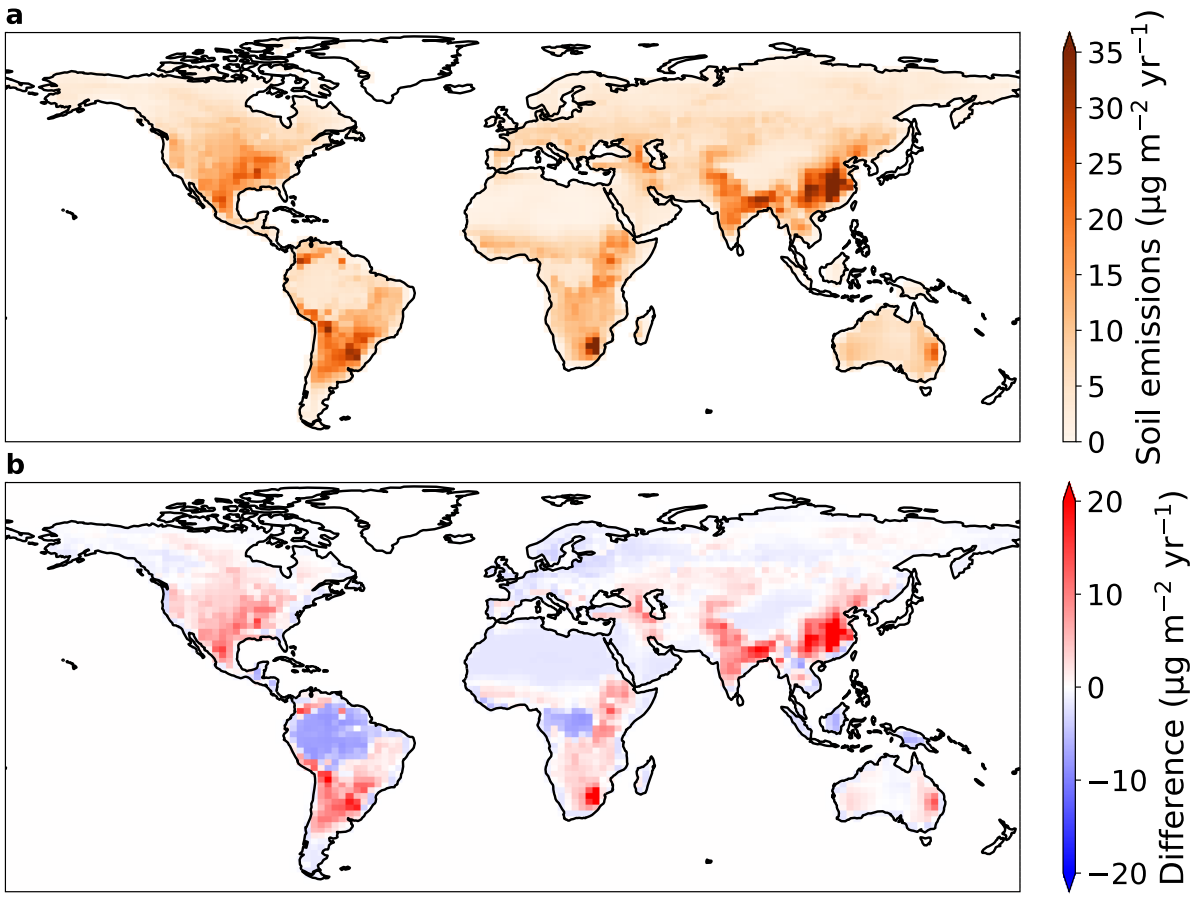

Figure S2. (*a*) Annual mean soil emissions of Hg^0 with the new parametrization. (*b*) Difference between new and old (GEOS-Chem v12.8) soil emissions parametrizations (new minus old).

Section S2. Observational constraints on deforestation Hg fluxes

There are several available sources of information that can be used to validate the deforestation emission factors (EF) calculated by GEOS-Chem (Fig. 1, SI Spreadsheet):

1) *Soil Hg concentration measurements of paired forest-deforested sites*:
Previous studies have measured the concentrations of Hg soils at deforested sites (C_d) and nearby forest (C_f) plots. For this analysis, we assume that the difference in these soil concentrations is due to mainly the change in atmospheric exchange, which is supported by the magnitude of modeled erosion fluxes (Section S6) and available measurements[5]. We use the following equation to convert the difference in these concentrations to a deforestation emission factor of Hg in Mg m^{-2} yr^{-1}:

$$\text{Total EF} = \frac{(C_d - C_f) \times \rho \times h}{t_d} \qquad \text{(S3)}$$

where ρ is the density of the soil, h is the depth of the soil layer, and t_d is the time since deforestation. In the US (Nearctic), there have been studies in Ohio[13] and Oregon[14] with measurements of Hg in deforested and forested soils, which we use to calculate deforestation EFs for the Nearctic. For the Amazon, more measurements are available (24 pairs of soil plots)[8–10,15–25]. We compiled a literature database of studies that compared Hg concentrations in deforested Amazonian soils with nearby forest plots (Fig. S3; SI Spreadsheet). Deforested sites show a consistent decrease compared to paired forested sites (p-value < 0.001; Wilcoxon signed-rank test), with the median decrease being 25 ng g^{-1} (10^{th}–90^{th} percentile: 2–58 ng g^{-1}). To calculate a deforestation EF for the Amazon, we apply this concentration decrease in Eq. S3 and assume an average Amazon soil density of 1.25 ng g^{-1}, a surface soil layer of 10 cm, and that deforested soils in the literature studies were measured 10 years after deforestation.

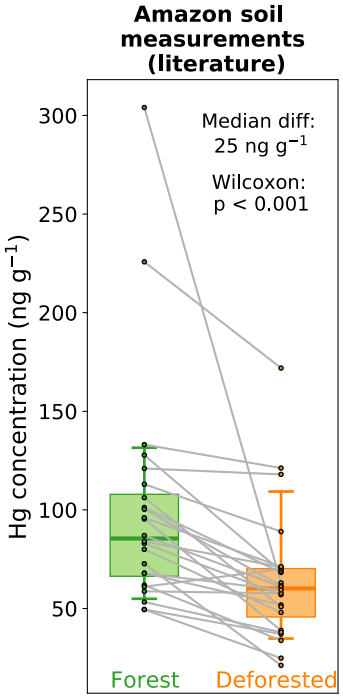

Figure S3. Measured Hg concentrations in forest (green) and deforested (orange) soils (0–20 cm depth) from the literature (n = 24)[8–10,15–25]. Box plots show the median values (solid lines), interquartile range (shaded), and 10th and 90th percentiles (whiskers). Gray lines connect paired sites from the same study. Listed p-value (<0.001) refers to the Wilcoxon signed-rank test of the null hypothesis that paired forest and deforested sites come from the same distribution.

2) *Terrestrial-atmosphere exchange models validated by Hg observations*:
An estimate for the deforestation EF over China is available from the Wang et al.[26] modeling study. We use their area-averaged mean fluxes over forest and agricultural land cover to calculate a deforestation emission factor:

$$\text{Total EF} = (E_d - D_d) - (E_f - D_f) \qquad \text{(S4)}$$

where E_d and E_f are the terrestrial emission fluxes (Mg m^{-2} yr^{-1}) from Chinese agricultural land and forest, and D_d and D_f are the deposition fluxes (Mg m^{-2} yr^{-1}) to Chinese agricultural land and forest. Although this EF estimate is model-based, the Wang et al.[26] model was validated extensively with available terrestrial-atmosphere exchange measurements from China.

3) *Dynamic flux chamber measurements of forested and deforested soils*:
Additional studies investigating the impact of deforestation on atmospheric fluxes quantified the response of soil emissions using dynamic flux chamber measurements[5,8–10,27,28]. We compare these measurements to the soil-only EF modeled by GEOS-Chem. The soil emission factors measured by the studies is calculated as the difference between soil emissions (Mg m^{-2} yr^{-1}) over deforested and forested soils:

$$\text{Soil EF} = E_d - E_f \qquad \text{(S5)}$$

The comparison between GEOS-Chem simulated deforestation EFs and observation-derived values is summarized in Fig. 1. Observations are only available from three regions (Amazon, China and Nearctic). We found further references investigating the impact of deforestation on Hg for the Palearctic region[29,30], yet these focused on measuring Hg concentrations in aquatic media and methylation potential rather than soil concentrations or atmospheric exchange. Australian soil measurements[31,32] have been made before and after vegetation burning events, but do not cover the longer term soil Hg response to deforestation.

The modeled EF estimates and their uncertainties overlap with observation-derived EFs for all 3 regions. If anything, the modeled best estimate used in online simulations is conservative compared to

available observations, showing generally lower EFs (Fig. 1). However, it is unclear whether the sparse observations available are representative of the overall region. The modeled EF uncertainty estimates cover 1–2 orders of magnitude, emphasizing the current uncertainties in the response of Hg fluxes to deforestation. Figure 1 also reveals the regions where no observations of the impact of deforestation on Hg cycling are currently available. Specifically, the Afrotropic and Indomalayan domains would be priorities for future measurement campaigns, given the current impact of deforestation in those regions (Fig. 2). It remains unknown whether Southeast Asian and African rainforests show similarly high levels of Hg in litterfall as the Amazon rainforest[33].

Section S3. Global deforestation-driven emissions estimates

We use perturbation simulations in which a set area within each region is deforested to calculate each deforestation EF. In the EF approach, we assume that 1) land-air fluxes respond linearly to deforested area and 2) spatial variability in the deforestation response within regions can be ignored. We explored the validity these assumptions using the four Amazon deforestation scenario simulations conducted in this work (Fig. S4). In the Amazon simulations — the reference simulation with 2003 forest cover (HIST), governance scenario for 2050 (GOV), business-as-usual for 2050 (BAU), and savannization (SAV) — different areas (both in spatial pattern and extent) were deforested in the Amazon region. The total fluxes from the Amazon basin for Hg^0 dry deposition, soil Hg^0 emissions, and the overall land-air balance of Hg all respond linearly ($R^2 > 0.98$) to the magnitude of the deforested area. Therefore, the approach of calculating deforestation EFs and scaling these with deforested areas would likely not be highly sensitive to the spatial distribution and amount of deforestation. Therefore, we conducted 7 other idealized deforestation simulations for the other land regions (Fig. S5).

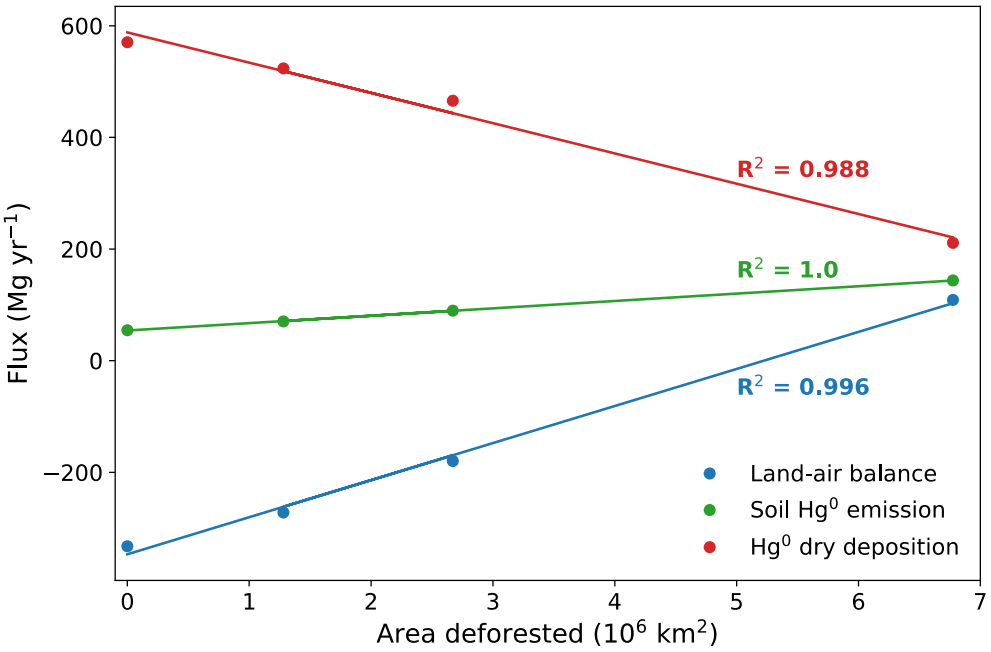

Figure S4. Relationship between land-air fluxes and the area deforested in GEOS-Chem simulations for the Amazon rainforest. Fluxes are averaged over the Amazon rainforest domain and listed R^2 values refer to linear models.

Additional data related to the calculation of historical deforestation-driven emissions of Hg are presented in this section. The maps defining the regions used in this study is shown in Fig. S5. Table S3 tabulates the results from the perturbation simulations for the different regions and the resultant emission factors. Fig. S6 explores the impact of choosing different time horizons for the deforestation area on the calculated Hg emissions globally and by country. Fig. S7 shows the map of Hg deforestation-driven emissions, assuming a 45 year time horizon (deforestation area of 1970–2014 from the LUH2 dataset[34]).

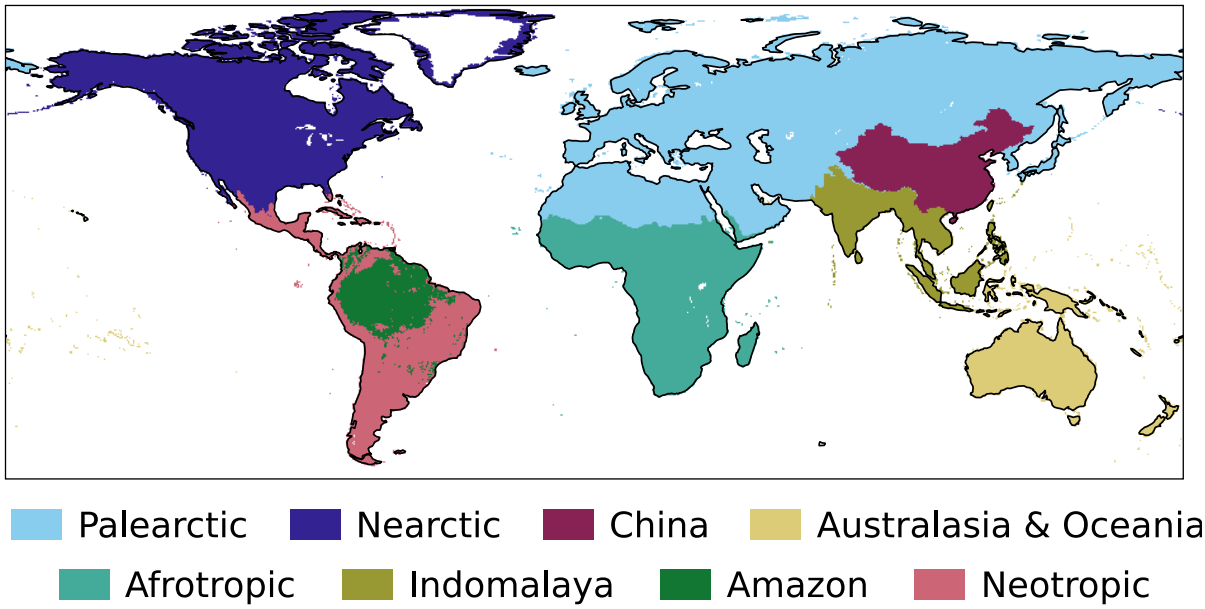

Figure S5. Definition of regions used to calculate the deforestation emission factors.

Table S3. Results from the deforestation perturbation simulations in GEOS-Chem for determining the response of land-air fluxes to deforesting a specified area. Emissions factors are listed with the 95% confidence interval calculated in offline simulations assessing the uncertainties due to model parameters (Section S4).

Realm	Area deforested (km^2)	Change in emissions ($Mg\ yr^{-1}$)	Change in deposition ($Mg\ yr^{-1}$)	Change in net emissions ($Mg\ yr^{-1}$)	Emissions factor ($Mg\ m^{-2}\ yr^{-1}$) [95% confidence interval]
Afrotropic	3 644 969	29.1	-10.0	39.1	1.1×10^{-5} [2.8×10^{-6} to 1.2×10^{-4}]
Neotropic	2 422 577	13.0	-4.9	17.9	7.4×10^{-6} [4.8×10^{-6} to 5.7×10^{-5}]
Indomalaya	2 626 474	31.6	-28.3	59.9	2.3×10^{-5} [1.5×10^{-5} to 2.1×10^{-4}]
Palearctic	4 221 663	5.8	-4.3	10.1	2.4×10^{-6} [7.6×10^{-8} to 2.3×10^{-5}]
Nearctic	4 606 898	31.6	-17.4	48.9	1.1×10^{-5} [7.1×10^{-6} to 6.2×10^{-5}]
Australasia	1 088 250	1.9	-4.8	6.6	6.1×10^{-6} [8.3×10^{-7} to 5.4×10^{-5}]
China	1 141 180	16.6	-10.1	26.7	2.3×10^{-5} [1.7×10^{-5} to 2.3×10^{-4}]
Amazon	6 775 429	96.2	-394.0	490.2	7.2×10^{-5} [4.5×10^{-5} to 2.0×10^{-4}]

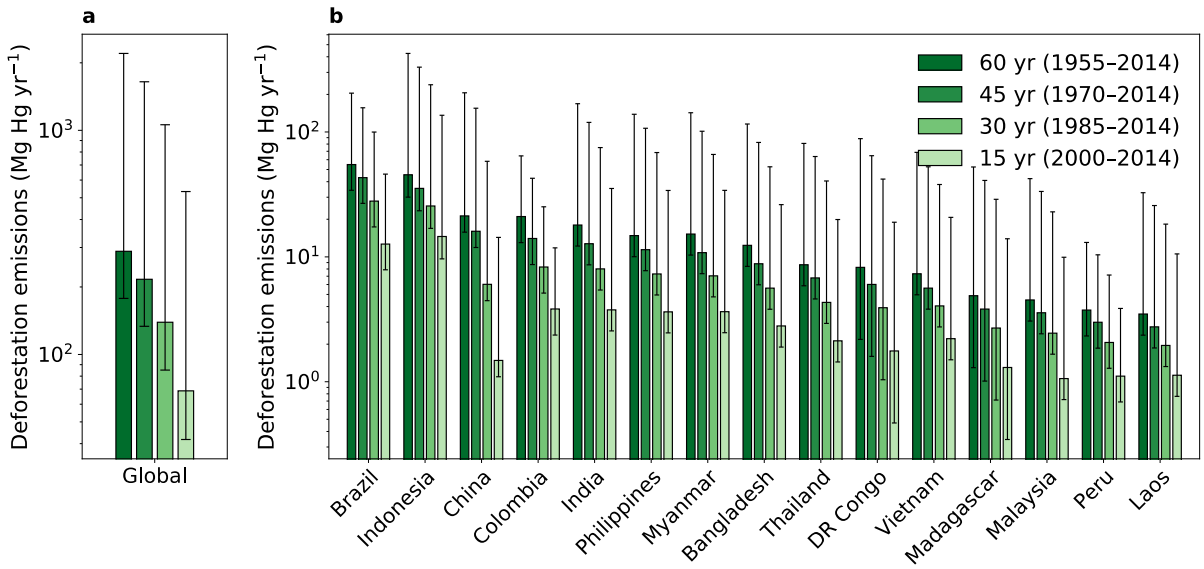

Figure S6. (*a*) Global and (*b*) country-level deforestation emissions of Hg for the top 15 emitting countries. Results are summarized accumulating deforested area over different time horizons (15 years, 30 years, 45 years, and 60 years) before 2015. Error bars refer to the 95% confidence interval based on the uncertainty in model parameters (Section S4).

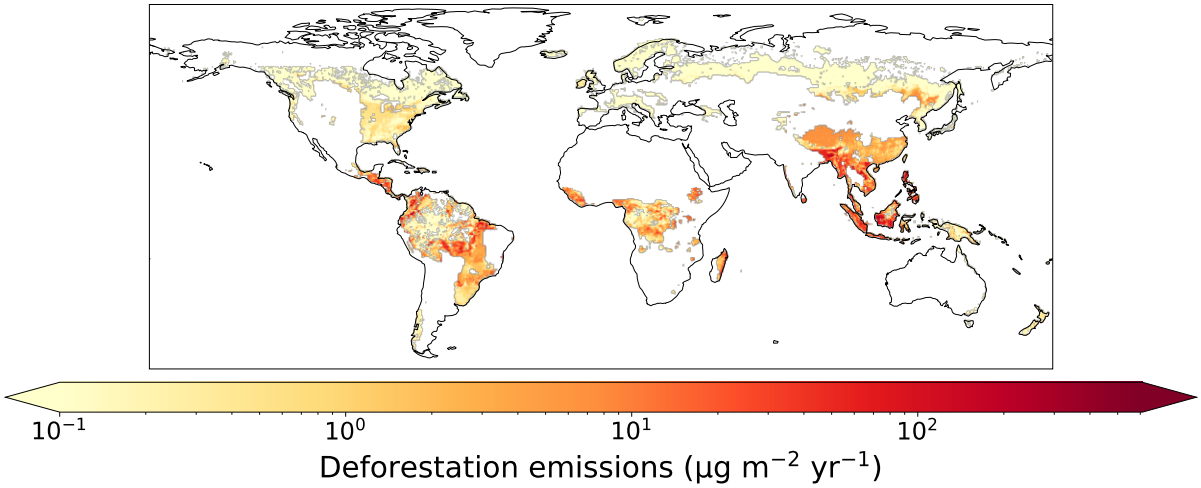

Figure S7. Map of net emissions of Hg from deforestation calculated over a 45 year time horizon before 2015 (1970–2014), using deforested area from the LUH2 dataset[34].

Section S4. Model uncertainty analysis

Table S4. Parameter uncertainty bounds applied in the uncertainty analysis.

Parameter	Min	Max	Units	Distribution	Comment
Soil emission parametrization	1	100	-	Uniform	Integer representing one of 100 reasonable parametrizations calculated within the range of observed uncertainties (Table S5)
Percentile of replaced LAI when building scenarios	10	90	-	Uniform	e.g., deforested Amazon area is assigned 10th percentile LAI of HIST savanna, instead of mean for default estimate
Dry deposition Hg^0 reactivity (f_0) Amazon rainforest	10^{-2}	0.5	-	Loguniform	Based on Feinberg et al.[33], within range of available vegetation uptake measurements
Dry deposition Hg^0 reactivity (f_0) other rainforests	10^{-5}	0.2	-	Loguniform	Based on Feinberg et al.[33]; no available measurements from other rainforests, leading to wider f_0 uncertainty
Dry deposition Hg^0 reactivity (f_0) elsewhere	10^{-5}	5×10^{-5}	-	Uniform	Based on Feinberg et al.[33], within range of available vegetation uptake measurements
Biomass burning emission factor for Amazon	350	615	μg m^{-2}	Uniform	Estimated range in literature[10,35,36]

Table S5. Bounds of observed parameters used to calculate 100 reasonable soil emission parametrizations, which are then applied in the uncertainty analysis (Table S4).

Parameter	Min	Max	Units	Comment
Ratio of deforested to forested Amazon soil emissions	1.8	31	-	Range from Table S1
Ratio of Amazon to extratropical soil emissions	3.5	8	-	Assume 50% error from Table S2
Extratropical grassland soil emissions	3.5	11.4	μg m^{-2} yr^{-1}	Grasslands and background soil range from literature reviews[6,7]
Deforested Amazon soil emissions	9.8	79	μg m^{-2} yr^{-1}	Range from Table S1

Section S5. Scenarios for Amazon deforestation and global reforestation

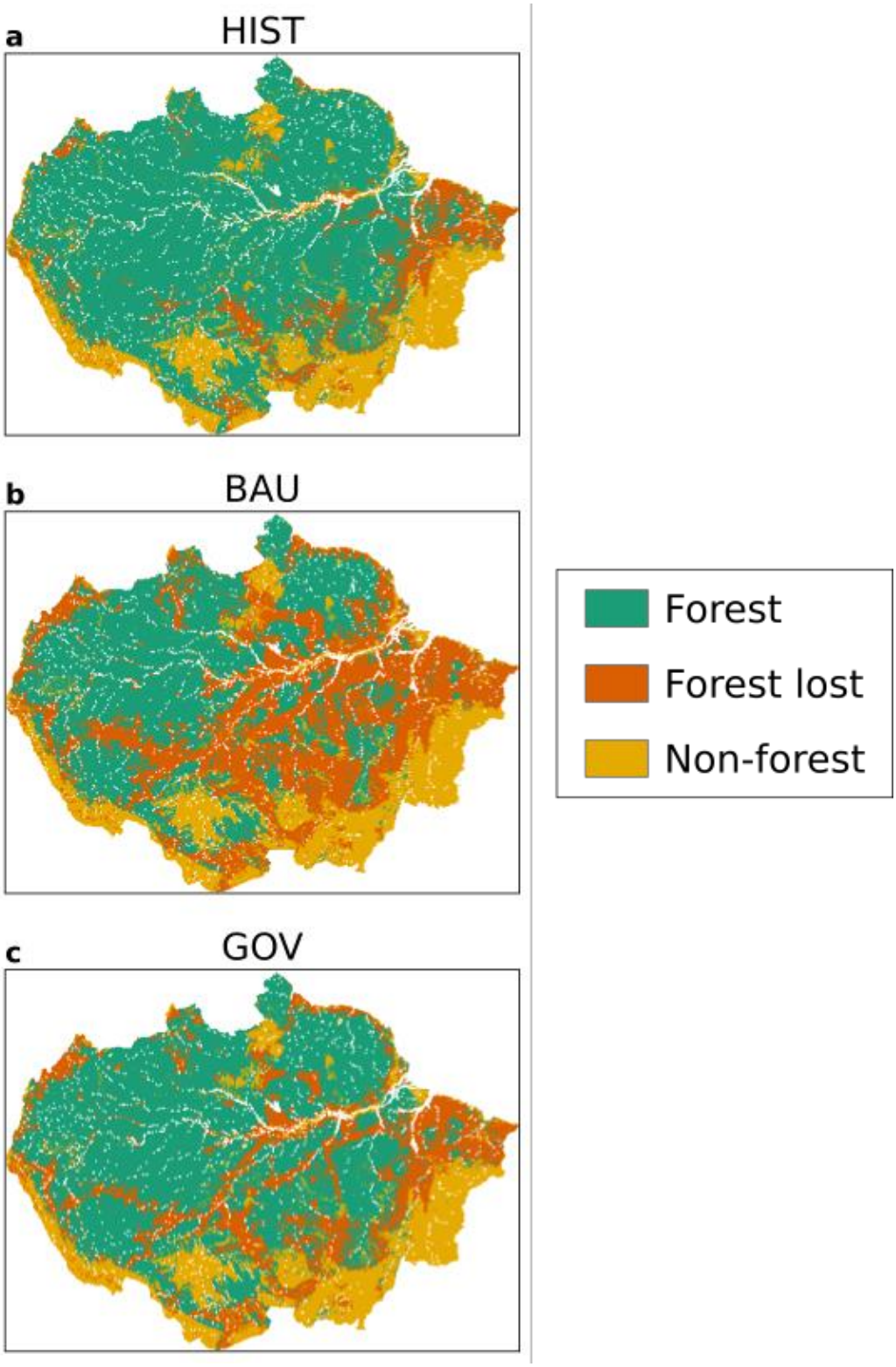

Figure S8. Map of the Amazon basin showing the area of forest, forest loss and rangeland and agriculture in (*a*) HIST; and projections for 2050 in (*b*) Business as Usual (BAU) and (*c*) Governance (GOV) scenarios (replotted from Soares-Filho et al.[37] data).

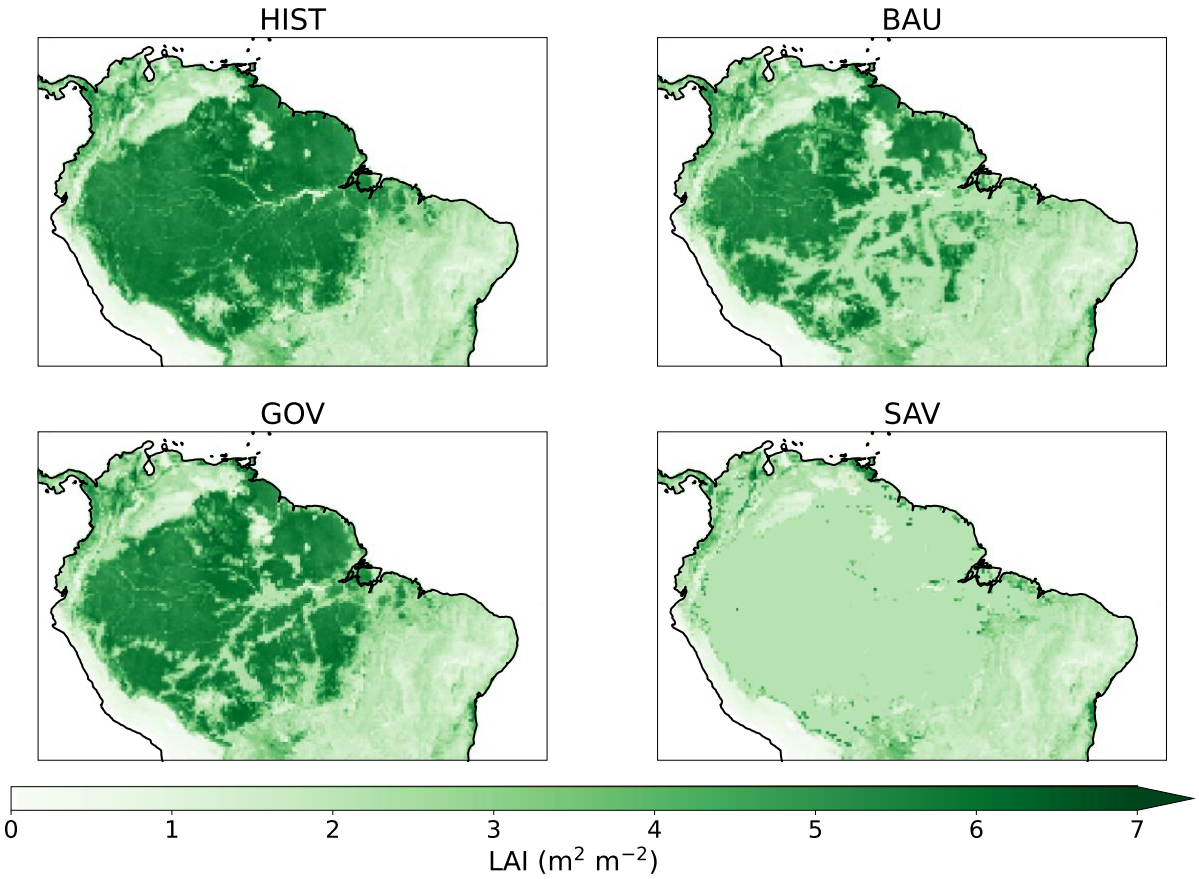

Figure S9. Annual mean leaf area index (LAI) maps for the Amazon deforestation scenarios at 0.25° × 0.25° resolution. The simulations names refer to the following scenarios: reference (HIST), Business-as-usual (BAU), Governance (GOV), and Savannization (SAV).

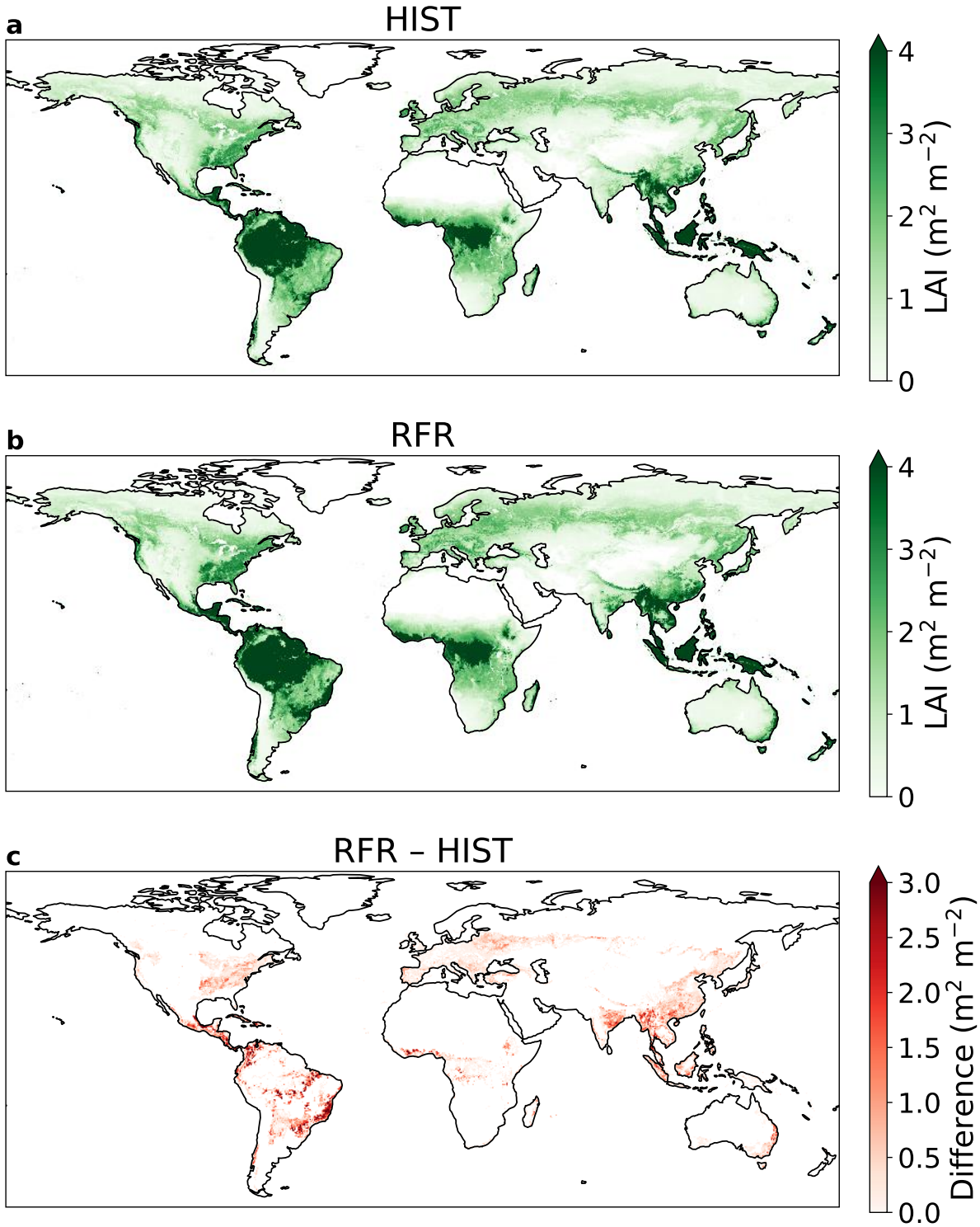

Figure S10. Annual mean leaf area index (LAI) maps at 0.25 × 0.25° resolution for: (*a*) the reference (HIST) scenario (*b*) Reforestation scenario (RFR) (*c*) Difference between RFR and HIST.

Section S6. Impact of Amazon deforestation on erosion

Previous field studies[15,38] have suggested that erosion of Hg is increased after deforestation in the Amazon, measuring enhanced runoff of Hg in deforested catchments. We estimated the change in soil displacement by water erosion (soil erosion) in the Amazon deforestation scenarios using the RUSLE-based[39] modeling platform Global Soil Erosion Modeling (GloSEM)[40,41]. As a detachment-limited soil erosion prediction model, GloSEM estimates soil erosion (expressed as a mass of soil lost per unit area and time, Mg ha^{-1} yr^{-1}) due to inter-rill and rill erosion processes by multiplication of six contributing

factors. The modeling scheme follows the same principle of most RUSLE-type models or more complex catchment-scale process-based models, with a driving force (erosivity of the climate, R), a resistance term (erodibility of the soil, K) and other factors representing the farming choice, i.e., topographical conformation of the field (LS), cropping system (C), and soil conservation practices (P).

Our approach for calculating soil erosion in the Amazon scenarios is similar to the GloSEM parametrization adopted by Borrelli et al.[40,41] to estimate human-induced soil erosion change between 2001 and 2070 at a global scale. The horizontal resolution of the native soil erosion modeling is 250 × 250 m. The calculation of erosivity (R), erodiblity (K), topographical conformation of the field (LS), and soil conservation practices (P) factors are described in Borrelli et al.[40,41]. We acknowledge that the calculation of erosion model factors for the Amazon rainforest may be associated with higher uncertainties than other regions due to the lower density in meteorological stations[42] and soil sampling sites[43]. For this study, we adapted the computation of the land cover and management factor (C-factor), which measures the combined effect of vegetation cover and cropping system variables on the soil erosion process. We parametrize the C-factor according to two layers of information: 1) the spatial dimension of land use classes according to the deforestation scenarios from Soares-Filho et al.[37] (described below); 2) the vegetation condition in each land use class using the MODIS MOD44B Vegetation Continuous Fields product (VCF) (~250m spatial resolution) as a proxy to quantify (i) surface vegetation cover, (ii) tree cover, and (iii) bare soil. As we focus our analysis on comparing the forest coverage in the years 2003 and 2050, the baseline vegetation condition is given by the average VCF values over the years 2000, 2001 and 2002. The C-factor for noncropland areas (C_{nc}) is estimated in two steps. First, a preliminary C-factor (C_p) not considering tree cover is calculated as:

$$C_p = C_{min} + \left((C_{max} - C_{min})\,\mathrm{NVS}\right) \quad \text{(S6)}$$

where the C_{min} (0.01) and C_{max} (0.15) express the potential range in C-factor values for dense to sparse grassland cover. NVS (non-vegetated surface) is spatially defined using the MODIS MOD44B VCF data normalized to a range from 0 to 1 and describes the percentage of ground covered by any vegetation type. For the NVS, the C-factor is set to 0.5. Within the next step, the final land cover and management C-factor for non-croplands (C_{nc}) is computed including the tree coverage (TC) defined using the MODIS MOD44B VCF normalized to range from 0 to 1:

$$C_{nc} = C_{p\,min} + \left(\left(C_{p\,max} - C_{p\,min}\right)\mathrm{TC}\right) \quad \text{(S7)}$$

where the $C_{p\,min}$ and $C_{p\,max}$ values are set to 0.0001 (100% canopy cover) and 0.009 (sparse forest vegetation).

While the deforestation scenarios proposed by Soares-Filho et al.[37] provide a spatial quantification of the forest losses between 2003 and 2050, the annual shares of conversion from forest to grassland or cropland are separate from the annual projection of the Land-Use Harmonization (LUH2) data[34], which provides fractional land-use patterns (850-2100) at 0.25° × 0.25° resolution. The downscaling of the LUH2 fractional cropland and grassland data from 0.25° × 0.25° resolution to the 250 m × 250 m resolution of the erosion model is performed through a probabilistic land use allocation scheme based on classification rules applied to auxiliary information (i.e., a crop suitability index, more detail in Borrelli et al.[40]). Finally, the C-factor of the cropland is defined at sub-national administrative level (Global Administrative Unit Levels) based on the Food and Agriculture Organization's (FAO) FAOSTAT database, which allowed to statistically describe typical crop rotations in each region. The C-factor of the croplands ranges from 0.131 (Northern Suriname) to 0.332 (Northeast Brazil).

Following the assumption of Lugato et al.[44] for eroded carbon, we assume that 30% of the eroded soil flux is not redeposited on land and enters riverine systems. The fraction of eroded Hg which enters aquatic systems is uncertain, depending on hillslopes dynamics and flow patterns that are not explicitly modeled by the RUSLE-based framework, as well as whether Hg would be selectively eroded relative to carbon. We recognize that this assumption introduces uncertainty into our calculations, and assume that the fraction of eroded soil which enters riverine systems can vary between 5–47%, the range reported by Van Oost et al.[45] We calculate the eroded flux of Hg from land by multiplying the soil flux by the median Hg concentration in Amazon forested soils from a literature review (86 ng g^{-1}; see SI Spreadsheet).

For each Amazon scenario, we tabulate the Hg erosion fluxes in Table S6. Erosion in the HIST scenario represents a flux of 64 Mg yr^{-1} (uncertainty range: 11–100 Mg yr^{-1}). Erosion is enhanced in the deforestation scenarios, ranging from +14% increase in GOV to a 96% increase in the extreme SAV scenario. The absolute magnitudes of erosion flux changes are smaller than the perturbations in the land-air flux, driven by changes in Hg^0 soil emissions and dry deposition (Table S6). Overall, perturbations to the erosion flux are approximately 14% of the perturbations to the land-air flux due to deforestation. A previous field study[5] has also suggested that the majority of flux changes after deforestation occurs through atmospheric exchange (97%) rather than erosion to riverine systems. Therefore, the land-air changes to the fluxes play the larger role in the impact of deforestation on the mass balance of Hg in soils. Nevertheless, changes to erosion will affect downstream Hg concentrations and the methylation potential after deforestation[5,29], which would be important to consider when assessing the impact of deforestation on local ecosystems.

Table S6. Soil erosion fluxes for the Amazon basin calculated by the erosion model GloSEM. The simulations names refer to the following scenarios: reference (HIST), Business-as-usual (BAU), Governance (GOV), and Savannization (SAV).

Scenario	**HIST**	**BAU**	**GOV**	**SAV**
Soil loss (Mt yr^{-1})	2467	3276	2816	4834
30% of soil loss (Mt yr^{-1})[a]	740	983	845	1450
[5%–47%]	[123–1159]	[164–1540]	[141–1323]	[242–2272]
Hg erosion (Mg yr^{-1})	64	85	73	125
[uncertainty range]	[11–100]	[14–132]	[12–114]	[21–195]
Change from HIST (Mg yr^{-1})	-	21	9	61
(relative change)		(+33%)	(+14%)	(+96%)
Land-air flux change from HIST (Mg yr^{-1})	-	153	61	441

[a] This is the flux assumed to be entering riverine systems

Section S7. Impacts on atmospheric Hg concentrations

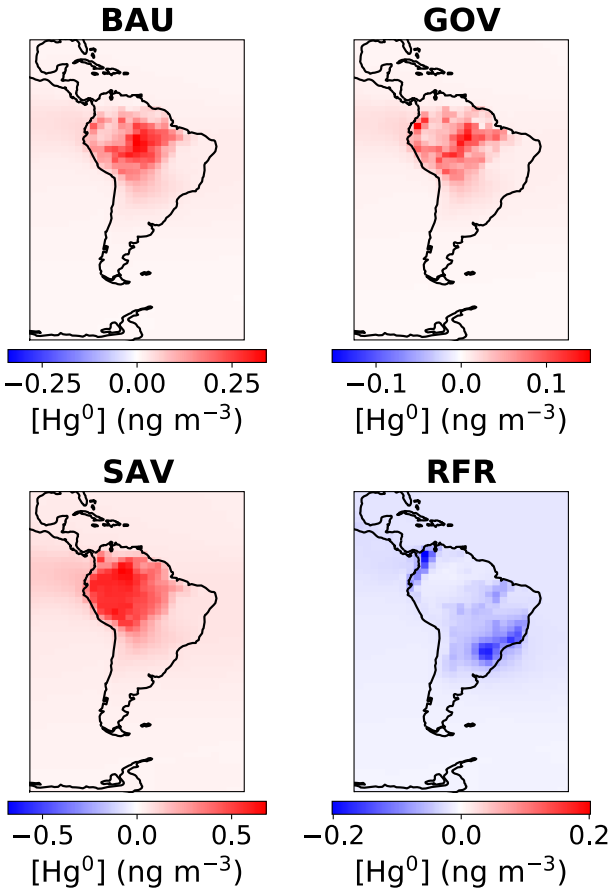

Figure S11. Annual mean differences in simulated atmospheric Hg^0 concentration at the surface between scenarios — Business-as-usual (BAU), Governance (GOV), Savannization (SAV), and global reforestation (RFR) — and the HIST reference simulation.

Supplementary References

(1) Khan, T. R.; Obrist, D.; Agnan, Y.; Selin, N. E.; Perlinger, J. A. Atmosphere-Terrestrial Exchange of Gaseous Elemental Mercury: Parameterization Improvement through Direct Comparison with Measured Ecosystem Fluxes. *Environ. Sci.: Processes Impacts* **2019**, *21* (10), 1699–1712. https://doi.org/10.1039/C9EM00341J.

(2) Selin, N. E.; Jacob, D. J.; Yantosca, R. M.; Strode, S.; Jaeglé, L.; Sunderland, E. M. Global 3-D Land-Ocean-Atmosphere Model for Mercury: Present-Day versus Preindustrial Cycles and Anthropogenic Enrichment Factors for Deposition. *Global Biogeochem. Cycles* **2008**, *22* (2), GB2011. https://doi.org/10.1029/2007GB003040.

(3) Verstraete, M. M. Radiation Transfer in Plant Canopies: Transmission of Direct Solar Radiation and the Role of Leaf Orientation. *J. Geophys. Res.* **1987**, *92* (D9), 10985. https://doi.org/10.1029/JD092iD09p10985.

(4) Zhou, J.; Wang, Z.; Zhang, X.; Driscoll, C. T.; Lin, C.-J. Soil–Atmosphere Exchange Flux of Total Gaseous Mercury (TGM) at Subtropical and Temperate Forest Catchments. *Atmos. Chem. Phys.* **2020**, *20* (24), 16117–16133. https://doi.org/10.5194/acp-20-16117-2020.

(5) Eckley, C. S.; Eagles-Smith, C.; Tate, M. T.; Krabbenhoft, D. P. Surface-Air Mercury Fluxes and a Watershed Mass Balance in Forested and Harvested Catchments. *Environmental Pollution* **2021**, *277*, 116869. https://doi.org/10.1016/j.envpol.2021.116869.

(6) Zhu, W.; Lin, C.-J.; Wang, X.; Sommar, J.; Fu, X.; Feng, X. Global Observations and Modeling of Atmosphere–Surface Exchange of Elemental Mercury: A Critical Review. *Atmos. Chem. Phys.* **2016**, *16* (7), 4451–4480. https://doi.org/10.5194/acp-16-4451-2016.

(7) Agnan, Y.; Le Dantec, T.; Moore, C. W.; Edwards, G. C.; Obrist, D. New Constraints on Terrestrial Surface–Atmosphere Fluxes of Gaseous Elemental Mercury Using a Global Database. *Environ. Sci. Technol.* **2016**, *50* (2), 507–524. https://doi.org/10.1021/acs.est.5b04013.
(8) Magarelli, G.; Fostier, A. Influence of Deforestation on the Mercury Air/Soil Exchange in the Negro River Basin, Amazon. *Atmos. Environ.* **2005**, *39* (39), 7518–7528. https://doi.org/10.1016/j.atmosenv.2005.07.067.
(9) Almeida, M. D.; Marins, R. V.; Paraquetti, H. H. M.; Bastos, W. R.; Lacerda, L. D. Mercury Degassing from Forested and Open Field Soils in Rondônia, Western Amazon, Brazil. *Chemosphere* **2009**, *77* (1), 60–66. https://doi.org/10.1016/j.chemosphere.2009.05.018.
(10) Carpi, A.; Fostier, A. H.; Orta, O. R.; dos Santos, J. C.; Gittings, M. Gaseous Mercury Emissions from Soil Following Forest Loss and Land Use Changes: Field Experiments in the United States and Brazil. *Atmos. Environ.* **2014**, *96*, 423–429. https://doi.org/10.1016/j.atmosenv.2014.08.004.
(11) Song, S.; Selin, N. E.; Soerensen, A. L.; Angot, H.; Artz, R.; Brooks, S.; Brunke, E.-G.; Conley, G.; Dommergue, A.; Ebinghaus, R.; Holsen, T. M.; Jaffe, D. A.; Kang, S.; Kelley, P.; Luke, W. T.; Magand, O.; Marumoto, K.; Pfaffhuber, K. A.; Ren, X.; Sheu, G.-R.; Slemr, F.; Warneke, T.; Weigelt, A.; Weiss-Penzias, P.; Wip, D. C.; Zhang, Q. Top-down Constraints on Atmospheric Mercury Emissions and Implications for Global Biogeochemical Cycling. *Atmos. Chem. Phys.* **2015**, *15* (12), 7103–7125. https://doi.org/10.5194/acp-15-7103-2015.
(12) Horowitz, H. M.; Jacob, D. J.; Zhang, Y.; Dibble, T. S.; Slemr, F.; Amos, H. M.; Schmidt, J. A.; Corbitt, E. S.; Marais, E. A.; Sunderland, E. M. A New Mechanism for Atmospheric Mercury Redox Chemistry: Implications for the Global Mercury Budget. *Atmos. Chem. Phys.* **2017**, *17* (10), 6353–6371. https://doi.org/10.5194/acp-17-6353-2017.
(13) Gamby, R. L.; Hammerschmidt, C. R.; Costello, D. M.; Lamborg, C. H.; Runkle, J. R. Deforestation and Cultivation Mobilize Mercury from Topsoil. *Science of The Total Environment* **2015**, *532*, 467–473. https://doi.org/10.1016/j.scitotenv.2015.06.025.
(14) Homann, P. S.; Darbyshire, R. L.; Bormann, B. T.; Morrissette, B. A. Forest Structure Affects Soil Mercury Losses in the Presence and Absence of Wildfire. *Environ. Sci. Technol.* **2015**, *49* (21), 12714–12722. https://doi.org/10.1021/acs.est.5b03355.
(15) Fostier, A. H.; Forti, M. C.; Guimarães, J. R.; Melfi, A. J.; Boulet, R.; Espirito Santo, C. M.; Krug, F. J. Mercury Fluxes in a Natural Forested Amazonian Catchment (Serra Do Navio, Amapá State, Brazil). *Sci. Total Environ.* **2000**, *260* (1–3), 201–211. https://doi.org/10.1016/S0048-9697(00)00564-7.
(16) Gerson, J. R.; Szponar, N.; Zambrano, A. A.; Bergquist, B.; Broadbent, E.; Driscoll, C. T.; Erkenswick, G.; Evers, D. C.; Fernandez, L. E.; Hsu-Kim, H.; Inga, G.; Lansdale, K. N.; Marchese, M. J.; Martinez, A.; Moore, C.; Pan, W. K.; Purizaca, R. P.; Sánchez, V.; Silman, M.; Ury, E. A.; Vega, C.; Watsa, M.; Bernhardt, E. S. Amazon Forests Capture High Levels of Atmospheric Mercury Pollution from Artisanal Gold Mining. *Nat Commun* **2022**, *13* (1), 559. https://doi.org/10.1038/s41467-022-27997-3.
(17) Almeida, M. D.; Lacerda, L. D.; Bastos, W. R.; Herrmann, J. C. Mercury Loss from Soils Following Conversion from Forest to Pasture in Rondônia, Western Amazon, Brazil. *Environmental Pollution* **2005**, *137* (2), 179–186. https://doi.org/10.1016/j.envpol.2005.02.026.
(18) Lacerda, L. D.; de Souza, M.; Ribeiro, M. G. The Effects of Land Use Change on Mercury Distribution in Soils of Alta Floresta, Southern Amazon. *Environmental Pollution* **2004**, *129* (2), 247–255. https://doi.org/10.1016/j.envpol.2003.10.013.
(19) Béliveau, A.; Lucotte, M.; Davidson, R.; do Canto Lopes, L. O.; Paquet, S. Early Hg Mobility in Cultivated Tropical Soils One Year after Slash-and-Burn of the Primary Forest, in the Brazilian Amazon. *Science of The Total Environment* **2009**, *407* (15), 4480–4489. https://doi.org/10.1016/j.scitotenv.2009.04.012.
(20) Béliveau, A.; Lucotte, M.; Davidson, R.; Paquet, S.; Mertens, F.; Passos, C. J.; Romana, C. A. Reduction of Soil Erosion and Mercury Losses in Agroforestry Systems Compared to Forests and Cultivated Fields in the Brazilian Amazon. *Journal of Environmental Management* **2017**, *203*, 522–532. https://doi.org/10.1016/j.jenvman.2017.07.037.
(21) Patry, C.; Davidson, R.; Lucotte, M.; Béliveau, A. Impact of Forested Fallows on Fertility and Mercury Content in Soils of the Tapajós River Region, Brazilian Amazon. *Science of The Total Environment* **2013**, *458–460*, 228–237. https://doi.org/10.1016/j.scitotenv.2013.04.037.

(22) Comte, I.; Lucotte, M.; Davidson, R.; Reis de Carvalho, C. J.; de Assis Oliveira, F.; Rousseau, G. X. Impacts of Land Uses on Mercury Retention in Long-Time Cultivated Soils, Brazilian Amazon. *Water Air Soil Pollut* **2013**, *224* (4), 1515. https://doi.org/10.1007/s11270-013-1515-3.

(23) Mainville, N.; Webb, J.; Lucotte, M.; Davidson, R.; Betancourt, O.; Cueva, E.; Mergler, D. Decrease of Soil Fertility and Release of Mercury Following Deforestation in the Andean Amazon, Napo River Valley, Ecuador. *Science of The Total Environment* **2006**, *368* (1), 88–98. https://doi.org/10.1016/j.scitotenv.2005.09.064.

(24) Roulet, M.; Lucotte, M.; Saint-Aubin, A.; Tran, S.; Rhéault, I.; Farella, N.; De Jesus Da silva, E.; Dezencourt, J.; Sousa Passos, C.-J.; Santos Soares, G.; Guimarães, J.-R. D.; Mergler, D.; Amorim, M. The Geochemistry of Mercury in Central Amazonian Soils Developed on the Alter-Do-Chão Formation of the Lower Tapajós River Valley, Pará State, Brazil. *Science of The Total Environment* **1998**, *223* (1), 1–24. https://doi.org/10.1016/S0048-9697(98)00265-4.

(25) Wasserman, J. C.; Campos, R. C.; Hacon, S. de S.; Farias, R. A.; Caires, S. M. Mercury in Soils and Sediments from Gold Mining Liabilities in Southern Amazonia. *Quím. Nova* **2007**, *30* (4). https://doi.org/10.1590/S0100-40422007000400003.

(26) Wang, X.; Lin, C.-J.; Yuan, W.; Sommar, J.; Zhu, W.; Feng, X. Emission-Dominated Gas Exchange of Elemental Mercury Vapor over Natural Surfaces in China. *Atmos. Chem. Phys.* **2016**, *16* (17), 11125–11143. https://doi.org/10.5194/acp-16-11125-2016.

(27) Mazur, M.; Mitchell, C. P. J.; Eckley, C. S.; Eggert, S. L.; Kolka, R. K.; Sebestyen, S. D.; Swain, E. B. Gaseous Mercury Fluxes from Forest Soils in Response to Forest Harvesting Intensity: A Field Manipulation Experiment. *Science of The Total Environment* **2014**, *496*, 678–687. https://doi.org/10.1016/j.scitotenv.2014.06.058.

(28) Ma, M.; Wang, D.; Sun, R.; Shen, Y.; Huang, L. Gaseous Mercury Emissions from Subtropical Forested and Open Field Soils in a National Nature Reserve, Southwest China. *Atmospheric Environment* **2013**, *64*, 116–123. https://doi.org/10.1016/j.atmosenv.2012.09.038.

(29) Eklöf, K.; Lidskog, R.; Bishop, K. Managing Swedish Forestry's Impact on Mercury in Fish: Defining the Impact and Mitigation Measures. *Ambio* **2016**, *45* (S2), 163–174. https://doi.org/10.1007/s13280-015-0752-7.

(30) De Wit, H. A.; Granhus, A.; Lindholm, M.; Kainz, M. J.; Lin, Y.; Braaten, H. F. V.; Blaszczak, J. Forest Harvest Effects on Mercury in Streams and Biota in Norwegian Boreal Catchments. *Forest Ecology and Management* **2014**, *324*, 52–63. https://doi.org/10.1016/j.foreco.2014.03.044.

(31) Abraham, J.; Dowling, K.; Florentine, S. Effects of Prescribed Fire and Post-Fire Rainfall on Mercury Mobilization and Subsequent Contamination Assessment in a Legacy Mine Site in Victoria, Australia. *Chemosphere* **2018**, *190*, 144–153. https://doi.org/10.1016/j.chemosphere.2017.09.117.

(32) Howard, D.; Macsween, K.; Edwards, G. C.; Desservettaz, M.; Guérette, E.-A.; Paton-Walsh, C.; Surawski, N. C.; Sullivan, A. L.; Weston, C.; Volkova, L.; Powell, J.; Keywood, M. D.; Reisen, F.; (Mick) Meyer, C. P. Investigation of Mercury Emissions from Burning of Australian Eucalypt Forest Surface Fuels Using a Combustion Wind Tunnel and Field Observations. *Atmospheric Environment* **2019**, *202*, 17–27. https://doi.org/10.1016/j.atmosenv.2018.12.015.

(33) Feinberg, A.; Dlamini, T.; Jiskra, M.; Shah, V.; Selin, N. E. Evaluating Atmospheric Mercury (Hg) Uptake by Vegetation in a Chemistry-Transport Model. *Environ. Sci.: Processes Impacts* **2022**, *24* (9), 1303–1318. https://doi.org/10.1039/D2EM00032F.

(34) Hurtt, G. C.; Chini, L.; Sahajpal, R.; Frolking, S.; Bodirsky, B. L.; Calvin, K.; Doelman, J. C.; Fisk, J.; Fujimori, S.; Klein Goldewijk, K.; Hasegawa, T.; Havlik, P.; Heinimann, A.; Humpenöder, F.; Jungclaus, J.; Kaplan, J. O.; Kennedy, J.; Krisztin, T.; Lawrence, D.; Lawrence, P.; Ma, L.; Mertz, O.; Pongratz, J.; Popp, A.; Poulter, B.; Riahi, K.; Shevliakova, E.; Stehfest, E.; Thornton, P.; Tubiello, F. N.; van Vuuren, D. P.; Zhang, X. Harmonization of Global Land Use Change and Management for the Period 850–2100 (LUH2) for CMIP6. *Geosci. Model Dev.* **2020**, *13* (11), 5425–5464. https://doi.org/10.5194/gmd-13-5425-2020.

(35) Michelazzo, P. A. M.; Fostier, A. H.; Magarelli, G.; Santos, J. C.; de Carvalho, J. A. Mercury Emissions from Forest Burning in Southern Amazon. *Geophys. Res. Lett.* **2010**, *37* (9), L09809. https://doi.org/10.1029/2009GL042220.

(36) Melendez-Perez, J. J.; Fostier, A. H.; Carvalho, J. A.; Windmöller, C. C.; Santos, J. C.; Carpi, A. Soil and Biomass Mercury Emissions during a Prescribed Fire in the Amazonian Rain Forest. *Atmospheric Environment* **2014**, *96*, 415–422. https://doi.org/10.1016/j.atmosenv.2014.06.032.

(37) Soares-Filho, B. S.; Nepstad, D. C.; Curran, L. M.; Cerqueira, G. C.; Garcia, R. A.; Ramos, C. A.; Voll, E.; McDonald, A.; Lefebvre, P.; Schlesinger, P. Modelling Conservation in the Amazon Basin. *Nature* **2006**, *440* (7083), 520–523. https://doi.org/10.1038/nature04389.

(38) Roulet, M.; Lucotte, M.; Farella, N.; Serique, G.; Coelho, H.; Passos, S.; Mergler, D. Effects of Recent Human Colonization on the Presence of Mercury in Amazonian Ecosystems. *Water Air Soil Pollut.* **1999**, *112*, 297–313.

(39) Renard, K. G.; Foster, G. R.; Weesies, G. A.; McCool, D. K.; Yoder, D. C. Predicting Soil Erosion by Water: A Guide to Conservation Planning with the Revised Universal Soil Loss Equation (RUSLE). *Agriculture handbook* **1997**, *703*.

(40) Borrelli, P.; Robinson, D. A.; Panagos, P.; Lugato, E.; Yang, J. E.; Alewell, C.; Wuepper, D.; Montanarella, L.; Ballabio, C. Land Use and Climate Change Impacts on Global Soil Erosion by Water (2015-2070). *Proc. Natl. Acad. Sci. U.S.A.* **2020**, *117* (36), 21994–22001. https://doi.org/10.1073/pnas.2001403117.

(41) Borrelli, P.; Robinson, D. A.; Fleischer, L. R.; Lugato, E.; Ballabio, C.; Alewell, C.; Meusburger, K.; Modugno, S.; Schütt, B.; Ferro, V.; Bagarello, V.; Oost, K. V.; Montanarella, L.; Panagos, P. An Assessment of the Global Impact of 21st Century Land Use Change on Soil Erosion. *Nat Commun* **2017**, *8* (1), 2013. https://doi.org/10.1038/s41467-017-02142-7.

(42) Panagos, P.; Borrelli, P.; Meusburger, K.; Yu, B.; Klik, A.; Jae Lim, K.; Yang, J. E.; Ni, J.; Miao, C.; Chattopadhyay, N.; Sadeghi, S. H.; Hazbavi, Z.; Zabihi, M.; Larionov, G. A.; Krasnov, S. F.; Gorobets, A. V.; Levi, Y.; Erpul, G.; Birkel, C.; Hoyos, N.; Naipal, V.; Oliveira, P. T. S.; Bonilla, C. A.; Meddi, M.; Nel, W.; Al Dashti, H.; Boni, M.; Diodato, N.; Van Oost, K.; Nearing, M.; Ballabio, C. Global Rainfall Erosivity Assessment Based on High-Temporal Resolution Rainfall Records. *Sci Rep* **2017**, *7* (1), 4175. https://doi.org/10.1038/s41598-017-04282-8.

(43) Hengl, T.; De Jesus, J. M.; MacMillan, R. A.; Batjes, N. H.; Heuvelink, G. B. M.; Ribeiro, E.; Samuel-Rosa, A.; Kempen, B.; Leenaars, J. G. B.; Walsh, M. G.; Gonzalez, M. R. SoilGrids1km — Global Soil Information Based on Automated Mapping. *PLoS ONE* **2014**, *9* (8), e105992. https://doi.org/10.1371/journal.pone.0105992.

(44) Lugato, E.; Smith, P.; Borrelli, P.; Panagos, P.; Ballabio, C.; Orgiazzi, A.; Fernandez-Ugalde, O.; Montanarella, L.; Jones, A. Soil Erosion Is Unlikely to Drive a Future Carbon Sink in Europe. *Sci. Adv.* **2018**, *4* (11), eaau3523. https://doi.org/10.1126/sciadv.aau3523.

(45) Van Oost, K.; Quine, T. A.; Govers, G.; De Gryze, S.; Six, J.; Harden, J. W.; Ritchie, J. C.; McCarty, G. W.; Heckrath, G.; Kosmas, C.; Giraldez, J. V.; Da Silva, J. R. M.; Merckx, R. The Impact of Agricultural Soil Erosion on the Global Carbon Cycle. *Science* **2007**, *318* (5850), 626–629. https://doi.org/10.1126/science.1145724.